SCIENTIFIC REPORTS

OPEN

Deep brain stimulation induces sparse distributions of locally modulated neuronal activity

Received: 20 September 2017
Accepted: 18 January 2018
Published online: 01 February 2018

YiZi Xiao[1], Filippo Agnesi[1], Edward M. Bello[1], Simeng Zhang[1], Jerrold L. Vitek[2,3] & Matthew D. Johnson[1,3]

Deep brain stimulation (DBS) therapy is a potent tool for treating a range of brain disorders. High frequency stimulation (HFS) patterns used in DBS therapy are known to modulate neuronal spike rates and patterns in the stimulated nucleus; however, the spatial distribution of these modulated responses are not well understood. Computational models suggest that HFS modulates a volume of tissue spatially concentrated around the active electrode. Here, we tested this theory by investigating modulation of spike rates and patterns in non-human primate motor thalamus while stimulating the cerebellar-receiving area of motor thalamus, the primary DBS target for treating Essential Tremor. HFS inhibited spike activity in the majority of recorded cells, but increasing stimulation amplitude also shifted the response to a greater degree of spike pattern modulation. Modulated responses in both categories exhibited a sparse and long-range spatial distribution within motor thalamus, suggesting that stimulation preferentially affects afferent and efferent axonal processes traversing near the active electrode and that the resulting modulated volume strongly depends on the local connectome of these axonal processes. Such findings have important implications for current clinical efforts building predictive computational models of DBS therapy, developing directional DBS lead technology, and formulating closed-loop DBS strategies.

Deep brain stimulation therapies, which employ high-frequency electrical stimulation, are known to modulate both neuronal firing rates and firing patterns in the stimulated nucleus, which in turn can disrupt pathological oscillatory activity and create complex informational lesions[1–3]. Such modulation motifs have been fairly well-characterized in the subthalamic nucleus and globus pallidus, which are two prominent DBS targets for Parkinson's disease, and where prominent inhibition and complex spike activity phase-locked to the stimulation pulse train have been reported[4–8]. Much less is known, however, about the cellular responses during HFS in the cerebellar-receiving area of motor thalamus, which is the primary DBS target for treating Essential Tremor (ET). There is also a general lack of knowledge on the whereabouts and distribution within various target nuclei of neurons whose firing activity has been modulated by DBS. Exploring these unknowns will enhance our collective capacity to design more targeted approaches to DBS therapies for a range of brain disorders.

Computational models have suggested that motor thalamic HFS regularizes thalamocortical neuron spike activity adjacent to the active electrode[9,10]. These stimulus-entrained activity patterns are thought to stem from a combination of regularizing ion channel dynamics and entrainment of synaptic signaling[11,12] by driving cerebellothalamic, corticothalamic, reticular nucleus, and thalamic interneuron afferents[13–17]. However, the relative synaptic innervation of afferents on motor thalamic neurons and the degree to which HFS affects each of these afferents[18,19] is not well understood. What is known from *in vivo* experiments is that HFS in the motor thalamus results in suppression of local oscillatory activity[20,21], generation of robust glutamate release[22], and accumulation of adenosine that can inhibit spike activity during stimulation[23,24].

The spatial distributions of neuronal firing rate and firing pattern changes around a thalamic DBS lead also have not been thoroughly investigated. Studies in other brain regions have suggested a sparse and long-range distribution of neuronal modulation within the stimulated nucleus. For instance, HFS at a 10 µA amplitude in the human globus pallidus internus was reported to suppress neuronal activity 250–600 µm away from the microelectrode tip[6], which is significantly greater than the predicted maximum modulated somatic distance

[1]Biomedical Engineering, University of Minnesota, Minneapolis, USA. [2]Neurology, University of Minnesota, Minneapolis, USA. [3]Institute for Translational Neuroscience, University of Minnesota, Minneapolis, USA. Correspondence and requests for materials should be addressed to M.D.J. (email: john5101@umn.edu)

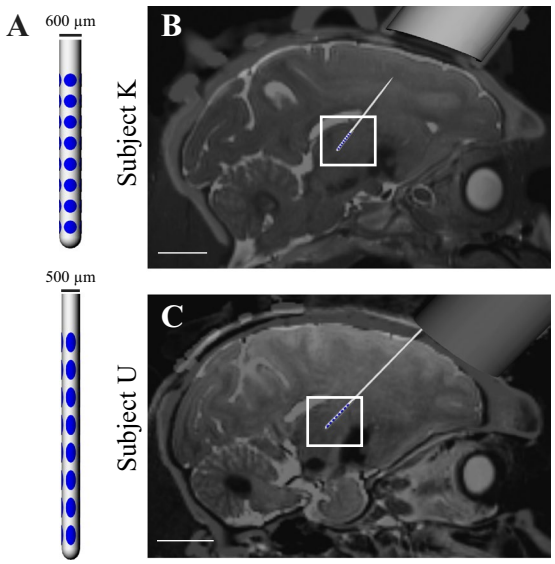

Figure 1. DBS Array Implants. (**A**) DBS arrays implantated in the cerebellar-receiving area of motor thalamus. (**B**,**C**) Co-registration of pre-operative T2-weighted MRI and post-implant CT images showing the final DBS array position and orientation in each subject. 1-cm scale bars are shown in (**B**,**C**).

based on first principles[25]. Such findings, as suggested in visual cortex[26], may stem from directly eliciting action potentials within local axonal processes that in turn connect with somata located distal to the active electrode. Similarly, given the complex network of interconnected neuronal processes within the motor thalamus, stimulation-induced modulation is likely to occur in a distributed manner, but this has not been thoroughly studied. In this study, we investigated the spatial context of motor thalamus spike activity to HFS in two healthy non-human primates chronically implanted with DBS arrays in the nucleus ventralis posterior lateralis pars oralis (VPLo), which is the homologue of the human DBS target for treating ET.

Materials and Methods

Animals. Two female rhesus macaque monkeys (*macaca mulatta*, Subject K and Subject U) were used in this study. All procedures were approved by the Institutional Animal Care and Use Committee of the University of Minnesota and were carried out in accordance with United States Public Health Service policy on the humane care and use of laboratory animals. The animals were given environmental enrichment, provided with water *ad libitum*, and given a range of food options including fresh fruit and vegetables. All efforts were made to provide good care and alleviate any discomfort for the animals during the study. Pre-operative 7T MRI was acquired at the Center for Magnetic Resonance Research at the University of Minnesota using a passively shielded 7T magnet (Magnex Scientific) for both animals. During the imaging sessions, the animals were anesthetized with isoflurane and monitored for depth of anesthesia. T2-W images were acquired with a 2D turbo spin echo sequence at 0.5 mm isotropic resolution using a field of view (FOV) of $128 \times 96 \times 48$mm[3,27]. In a separate procedure, under isoflurane anesthesia, each animal was surgically implanted with a titanium headpost (Gray Matter Research) and a cephalic chamber (Crist Instruments) oriented in the parasagittal plane with an off-vertical angle of 31.0° in Subject K and 38.5° in Subject U. Each animal also received a post-implant CT scan to plan the DBS lead implantation using *Monkey Cicerone*[28].

DBS implant procedure. Microelectrodes (250 µm shank diameter, 0.8–1.2 MΩ, FHC) were advanced through the chamber under the guidance of *Monkey Cicerone* to map the boundaries of VPLo. A combination of unit-spike responses to passive joint manipulation and microstimulation-evoked movements at thresholds less than 50 µA were used to identify VPLo and its borders[29]. The monopolar microstimulation parameters included a 0.5 second, 300 Hz train of biphasic, charge-based waveforms with a 100 µs cathodic phase, 20 µs interphase interval, and 100µs anodic phase. All monopolar stimulation settings applied for mapping and subsequent DBS experiments used a Gray Matter Research titanium headpost with bilaterally distributed titanium bone screw anchors over the parietal and occipital cranial regions as the return electrode. For each subject, the mapping track that yielded a long stretch of VPLo was chosen for chronic implantation of a DBS array. A radially segmented DBS array[30] (NeuroNexus, Fig. 1A) with 32 ellipsoidal macroelectrodes (8 rows × 4 columns) arranged around a 600 µm diameter (Subject K) or 500 µm diameter shaft was chronically implanted into the VPLo through the pre-planned track. In Subject K, macroelectrodes had dimensions of 360 × 360 µm with 572 µm center-to-center distance between rows. In Subject U, macroelectrode sites were 280 µm wide × 530 µm tall with 750 µm center-to-center distance between rows. All electrodes were independent channels, electrically insulated from each other. Following DBS array implantation, a post-operative CT scan was performed to visualize the implantation trajectory, depth, and orientation of the DBS array using *Monkey Cicerone*. Each DBS array assembly had a flexPCB cable extending from the lead body within the cranial chamber. This assembly served as a fiducial marker for electrode column alignment along the lead shank. Prior to implantation, the DBS arrays were inspected under

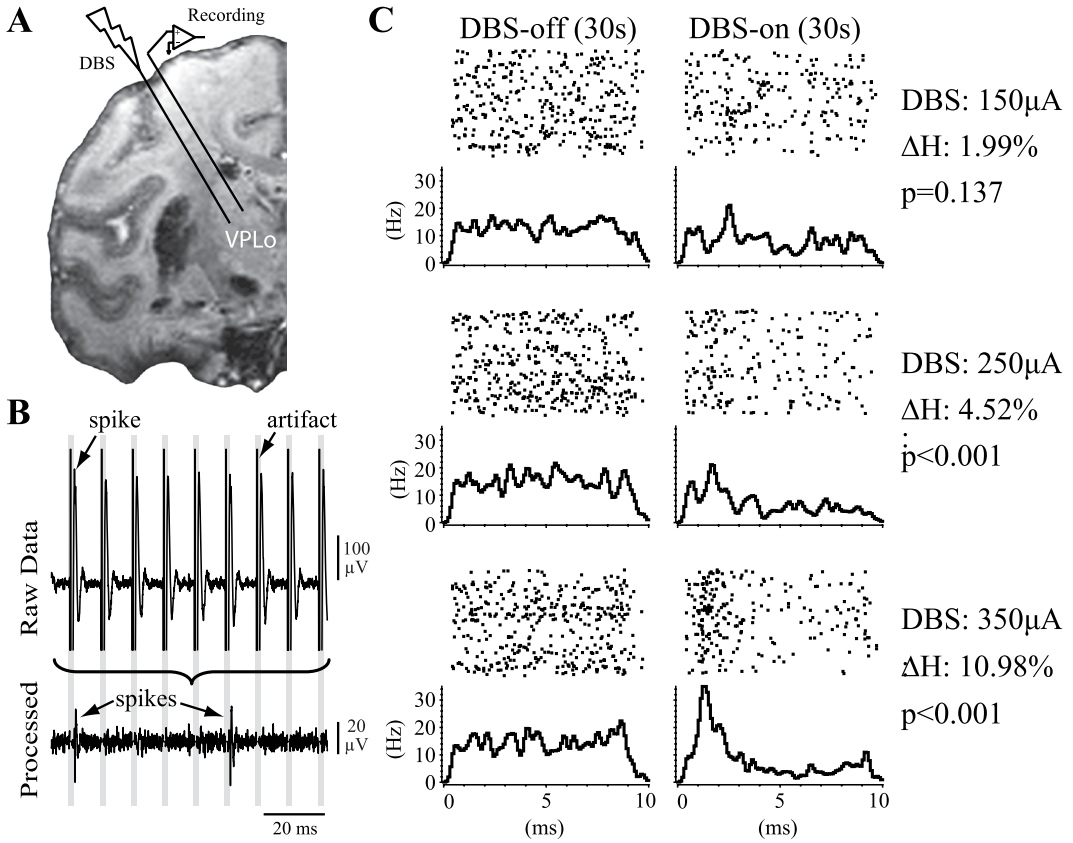

Figure 2. Single-unit spike recording analysis in the context of VPLo-HFS. (**A**) Microelectrode recordings were performed in the cerebellar receiving area of thalamus (VPLo) while stimulating in the same thalamic nucleus. (**B**) Recording artifacts were template-subtracted, with stimulation times used to generate peristimulus time histograms (PSTHs) of spike activity. Spike depolarization is shown as a negative polarity. (**C**) PSTHs from a recorded neuron before and during HFS at three different stimulation amplitudes. ΔH is the percentage decrease in PSTH entropy between the HFS-off and HFS-on states. The p value indicates the likelihood of the observed PSTH entropy during HFS to occur by chance.

the microscope to confirm this alignment. The preoperative T2-W images were then co-registered with the post-operative CT to determine the DBS array position within the VPLo (Fig. 1B,C).

DBS protocols. To visually assess the existence and in turn magnitude of stimulus-evoked motor twitches consistent with stimulation in the VPLo[29], current controlled stimulation with parameters identical to those used during mapping was delivered through each electrode. The row of electrodes with the lowest threshold response for evoking a transient muscle contraction was chosen for stimulation and used in the microelectrode recording experiments in each animal (fourth row from the bottom in Subject K and the bottom row in Subject U). These muscle twitches were not sustained during longer duration stimulation trials. For subsequent recording experiments, a stimulus train at 100 Hz waveforms (charge-balanced and identical to those used for mapping) was delivered using a randomized presentation of three stimulus amplitudes (150, 250, and 350 μA) at each of the four electrodes along the selected row. At these stimulation frequencies and amplitudes, stimulus-induced muscle twitches were not observed and no motor deficits or other behavioral abnormalities were apparent. Current-controlled stimulation was used to reduce the propensity for *in vivo* impedance-based voltage fluctuations in tissue observed with constant voltage stimulation[31]. Current density at the stimulated electrode was 3.55 mA/mm^2, which is higher than what has been used in ET patients (~0.39 mA/mm^2)[32], but is lower in overall peak current intensity (0.35 mA in this study, and 2.58 mA in humans, a factor of 7.4). This, however, must be put in context that the human cerebellar-receiving area of thalamus is approximately 8.2 times larger than the thalamic cerebellar-receiving area of in the rhesus macaque[33,34]. The tested amplitudes (150–350 μA) ensured electrode current densities also were within safe limits given the relatively smaller dimensions of the electrodes.

Extracellular recordings. At least three weeks after DBS array implantation, stiff, epoxy dip-coated tungsten microelectrodes (250 μm shank diameter, 0.8–1.2MΩ, FHC) were inserted acutely around the chronically implanted DBS array in each animal (Fig. 2A). Wide-band recordings from these microelectrodes were digitized at 44 kHz (Alpha Omega SNR). Recordings were performed in the resting state before (30–60 s), during (60 s), and after HFS (30–60 s). Single-unit spike activity was recorded from 85 cells in Subject K (21 recording tracks) and 97 cells in Subject U (11 recording tracks). Extracting unit-spike activity involved filtering the data between

400–9000 Hz and removing stimulation artifacts using a template subtraction procedure[1,35] (Fig. 2B). This process reduced the period of recording obscured by stimulation artifacts to a small blanked period (average ~0.5 ms). To prevent biasing the data, similarly blanked regions were introduced in the pre- and post-HFS recording epochs using "virtual stimulation" timestamps at the same stimulation pulse frequency. Template-subtracted spike recordings were thresholded and sorted in Offline Sorter (Plexon) to identify unit-spike activity and to verify that isolation of a single unit did not have spikes within a 2 ms refractory period. All recordings were selected based upon their good isolation characteristics through the spike sorting process. While most neuronal recordings were stable enough to record effects of HFS through each of the four radial electrodes at three different amplitudes (12 recordings in total), it was not possible to achieve this with every neuron (n = 135/182 were recorded across all configurations in both animals).

Statistical Analyses. Time-stamps of spike activity, stimulation pulses, and virtual stimulation pulses were used to generate peri-stimulus time histograms (PSTHs, NeuroExplorer) (0.1 ms bins) before, during, and after HFS to visualize the degree of entrainment in spike activity to stimulation (or virtual stimulation) (Fig. 2C). PSTH comparisons between stimulation off/on conditions used the pre-HFS and HFS data, respectively, while visual inspection of the post-HFS data were used to verify that the unit-spike waveform shape and amplitude remained stable throughout the entire recording session. The post-HFS data will be reported in a follow-up study comparing neuronal activity within multiple DBS targets during the wash-out period after HFS. In terms of PSTH analysis, previous studies have used either thresholding[36] or cumulative sum[37] methods to determine instances of significant firing pattern modulation in PSTHs. However, these statistical methods do not quantify the gradual and often subtle changes in HFS-induced firing pattern modulation that are present within PSTHs. For this study, an entropy-based method was developed to quantify the degree of change in PSTHs between the off (immediately before HFS onset) and on (during HFS) states. Studies in the past have also used entropy as a quantitative measure of neuronal spike activity. However, the focus of these methods was to either measure neuronal information from inter-spike intervals[38–40] or spike train data[41]. We considered entropy (H) of a PSTH and computed this variable using the following equation based on the frequentist interpretation[42]

$$H(x) = \sum_{i=1}^{m} p(x_i) log \frac{1}{p(x_i)} \quad (1)$$

where m is the number of bins in the PSTH, x_i is the total number of spikes that fell into PSTH bin i and $p(x_i)$ is the relative frequency that a spike falls into PSTH bin i. This formulation of PSTH entropy dictates that entropy will be high when spikes fall randomly within the inter-stimulus pulse period (i.e. a flat PSTH), and will be lower when stimulus-locked activity (i.e. peaks or troughs in the PSTH) occurs. The bin size in equation (1) was chosen to be 0.5 ms, consistent with the shortest observed interval of entrained spike responses in the PSTH when considering a very narrow bin size. Bin sizes that were too narrow or too broad deprived equation (1) of the power to capture a decrease in H. The first 0.5 ms in each PSTH was excluded from analysis to avoid false positives related to the blanking period from the stimulus subtraction algorithm. Excitatory or inhibitory firing pattern modulation manifested as a drop in H between HFS-off and HFS-on periods as calculated by:

$$\Delta H\% = \frac{H_{HFS\_off} - H_{HFS\_on}}{H_{HFS\_off}} \times 100\% \quad (2)$$

Statistical significance of firing pattern modulation was determined by sampling with replacement n spikes from the HFS-off period (where n equals the total number of spikes in the HFS-on period); calculating H using equation (1); repeating this process 10,000 times to generate a bootstrapped distribution of HFS-off PSTH entropies (H_{HFS_off}); and, computing the HFS-on PSTH entropy (H_{HFS_on}). Statistically significant firing pattern modulation was defined by cases when the bootstrapped H_{HFS_off} distribution was less than H_{HFS_on} with a probability less than 5% ($\alpha = 0.05$) (Fig. 2C). Firing rates calculated before, dur_ing, and after HFS were also compared for each recorded cell. A statistically significant difference in firing rate was established using the Mann-Whitney U test (1 s bins, $p < 0.01$). Significant excitatory firing pattern modulation or firing rate increase were designated as 'p+' and 'r+', respectively, while significant inhibitory firing pattern modulation or firing rate decrease were designated as 'p−' and 'r−'. No significant change in any of the above categories was designated as 'n'. A small fraction of recordings (<2%) were observed to have intermittent and very sparse spike activity (<1 Hz) in either the HFS-off or HFS-on periods, which led to inaccurate representations of the PSTH entropy. These recordings were excluded from further analysis. The datasets generated and analyzed during the current study are available from the corresponding author on reasonable request.

To contextualize the spatial distribution of the PSTH results, two methods were used. The first involved charting the putative locations of microelectrode recordings defined through the microdrive relative to the CT localization of the DBS array. The Narishige microdrive, used for the microelectrode recording experiments, provided a snug fit for the insertion guide tube to puncture the trajectory of the microelectrode during insertion. Coordinates for implantation were determined using the Narishige x-y positioner, which had an x-y spatial resolution of 100 µm and depth resolution of 10 µm. In the second case, the size of the monopolar stimulus artifact recorded from the microelectrode was used as a proportional measure of distance, according to volume conductor theory[43,44]. For each recording session, the artifacts from stimulation amplitudes (150, 250, or 350 µA) were each averaged, and the peak magnitude (mV) of the recorded waveform was used as the pseudo measure for distance. Neuronal recordings were then assigned based on observations that neurons generally need to be within 50 μm of a microelectrode in order to be reliably identified in the spike sorting process[45,46].

Results

Heterogeneity of Neuronal Responses to HFS in the VPLo. Thalamic responses to HFS exhibited firing rate and/or firing pattern modulation in both subjects (Fig. 3A–F). A total of 65.5% (54/85) and 74.2% (72/97) of the recorded cells in Subject K and Subject U, respectively, showed exclusively firing rate modulation for one or more of the stimulation amplitudes and electrode configurations (up to 4 electrodes × 3 amplitudes = 12 instances of HFS for a given cell). Additionally, 12.9% (11/85) and 21.7% (21/97) of the recorded cells in Subject K and Subject U, respectively, exhibited firing pattern modulation (p+ or p−) that may or may not have also included firing rate modulation (e.g. p+r+, p+r−, p−r+, or p−r−) during HFS.

The recordings were subsequently grouped by stimulation amplitude and divided into nine categories that included spike activity phase-locked to the stimulus pulse with either excitatory or inhibitory entrainment as well as overall changes in firing rate with both excitatory and inhibitory effects (Fig. 3G–J). Of the recordings that exhibited modulation of spike activity, the percentage of responsive recordings increased modestly from 19% at 150 µA to 26% at 350 µA in Subject K and from 43% at 150 µA to 46% at 350 µA in Subject U. More notably, however, for recordings showing modulation to HFS, there was a shift from primarily firing rate modulation to a more diverse collection of firing rate and firing pattern responses. More specifically, 'r+' and 'r−' responses accounted for 88% and 56% of all responsive recordings at 150 and 350 µA, respectively, in Subject K. Similarly, the proportion of firing rate modulation responses was 94% at 150 µA and 80% at 350 µA in Subject U. This decrease was balanced by an increase in the proportion of firing pattern modulation responses in that the majority of cells exhibiting firing pattern modulation at any of the stimulus amplitudes transitioned from no modulation or only rate modulation at lower stimulus amplitudes to pattern modulation with or without rate modulation at higher stimulus amplitudes (Fig. 3K,L).

Neuronal Pattern Responses as a Function of Stimulus Amplitude. The strength of firing pattern modulation, as a function of stimulus amplitude, was further investigated. Only those recording sessions that underwent HFS at all three amplitudes (150, 250, and 350 µA) were included in this analysis. The recordings were grouped into two categories: HFS failed to elicit firing pattern modulation (i.e. 'n', 'r+' and 'r−') at any of the three stimulation amplitudes (Group nFPM), and HFS elicited firing pattern modulation (i.e. 'p+', 'p−', 'p+r+', 'p+r−', 'p−r+' and 'p−r−') with at least one stimulation amplitude (Group FPM). Subject K had 224 and 21 recordings in Groups nFPM and FPM, respectively. Subject U had 251 and 32 recordings in Groups nFPM and FPM, respectively.

Within each group, one-way ANOVA was performed to test for a significant difference ($\alpha = 0.05$) in the average ΔH% with stimulus amplitude as the explanatory variable. A significant difference was found in Group FPM for both animals (Subject K: $p = 0.028$, Subject U: $p = 0.021$), but not Group nFPM for both animals (Subject K: $p = 0.276$, Subject U: $p = 0.247$). Multiple-comparison tests ($n = 3$, Mann-Whitney U test with Bonferroni correction, $\alpha = 0.05/3 = 0.0167$) were subsequently performed on the data in Group FPM. In both animals, significant differences were found between the 150–350 µA groups and the 250–350 µA groups, but not between the 150–250 µA groups (Fig. 4A,B). The analysis also showed that firing pattern modulation was more likely to occur at higher stimulus amplitudes, and more specifically, the 350 µA case, which accounted for 48% and 41% of all recordings with firing pattern modulation in Subject K and U, respectively (Fig. 4C).

Distribution of Neuronal Firing Pattern Modulation around the DBS Array. The spatial distribution of modulated activity within motor thalamus was investigated in two contexts (Fig. 5). First, recording site locations were estimated generally from co-registration of the microdrive coordinate system with the post-operative CT scan, which showed both microdrive and array implant positions and orientations. For this spatial analysis, recording site locations were considered to have a firing pattern change if any of the stimulation amplitudes or electrode configurations induced a statistically significant firing pattern change. Most recording site locations exhibited only firing rate modulation with locations both proximal and distal to the row of active electrodes. Recording site locations with no modulation occurred at more distal locations relative to the active electrodes. Recording site locations in which firing pattern modulation, with or without firing rate modulation, were also distributed around and along the DBS array. Notably, recording site locations immediately adjacent to one another were found to exhibit firing rate modulation but no firing pattern modulation, and vice versa.

Additionally, the average peak stimulus artifact amplitude was used as a pseudo-measure of distance between the active stimulating electrode and the microelectrode recording the neuronal spike activity. Stimulus artifact amplitude was related to stimulus-induced firing pattern changes in a total of 783 and 872 recordings in Subject K and Subject U, respectively, with each recording corresponding to HFS with a single stimulus amplitude. PSTHs were created for each recording, and the $\Delta\mathbf{H}$**%** between the HFS-off and HFS-on epochs was calculated and plotted against the peak stimulus artifact amplitude (Fig. 6A,B). Similar to the microdrive-based calculations, a distributed and sparsely populated spatial profile of firing pattern modulation was observed. Instances of significant firing pattern modulation occurred over a wide range of stimulus artifact amplitudes and changes in PSTH entropy. The data also showed that recordings with either firing rate or firing pattern modulation responses to HFS had spatially distributed profiles in both subjects without a clear difference in the median stimulation artifact amplitude (Fig. 6C,D). The relationship between the stimulus artifact amplitude and the estimated recording site distance (d) was consistent with a nonlinear decay function that was proportional to $1/d^x$ (Fig. 6E,F). Nonlinear curve fitting resulted in estimates for x as 0.36, 0.31, and 0.32 for the 350, 250, and 150 µA stimulus intensities in Subject K, respectively, and for x as 0.42, 0.42, and 0.40 for the 350, 250, and 150 µA stimulus intensities in Subject U, respectively. The coefficient of determination (R^2) for these curve fits ranged between 0.17–0.23 for Subject K and between 0.33–0.36 for Subject U.

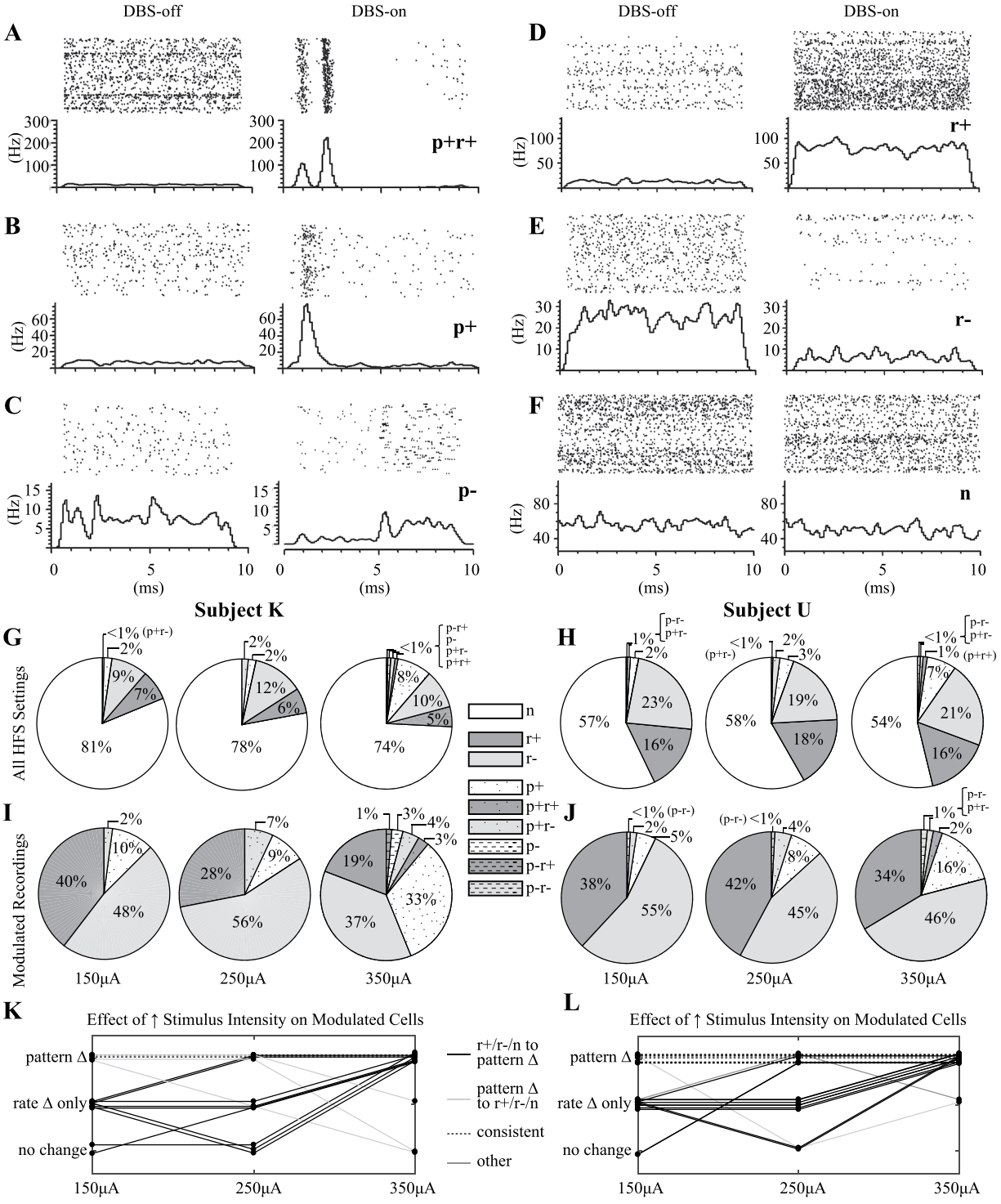

Figure 3. Heterogeneity of thalamic PSTH responses to VPLo-HFS with increasing stimulation amplitude. (**A**–**F**) Representative examples of the following classes of responses (p: firing pattern modulation, r: firing rate modulation. '+': increase in firing rate or phase-locked spike activity, '−': decrease in firing rate or phase-locked spike activity, n: no response). (**G**–**J**) Dependence of stimulation amplitude on motor thalamic neuronal responses to VPLo-HFS. Data from Subject K and Subject U are on the left and right side of the legend, respectively. The top row shows the proportionate effects of HFS at 150, 250, and 350 μA across all recordings (Subject K: n = 245, Subject U: n = 283), whereas the bottom row shows the corresponding percentages only for those recordings that were significantly modulated by HFS (i.e. firing pattern or rate modulation). (**K,L**) Effect of stimulus amplitude on all cells exhibiting one or more instances of firing pattern modulation (n = 11 cells in Subject K, n = 21 cells in Subject U).

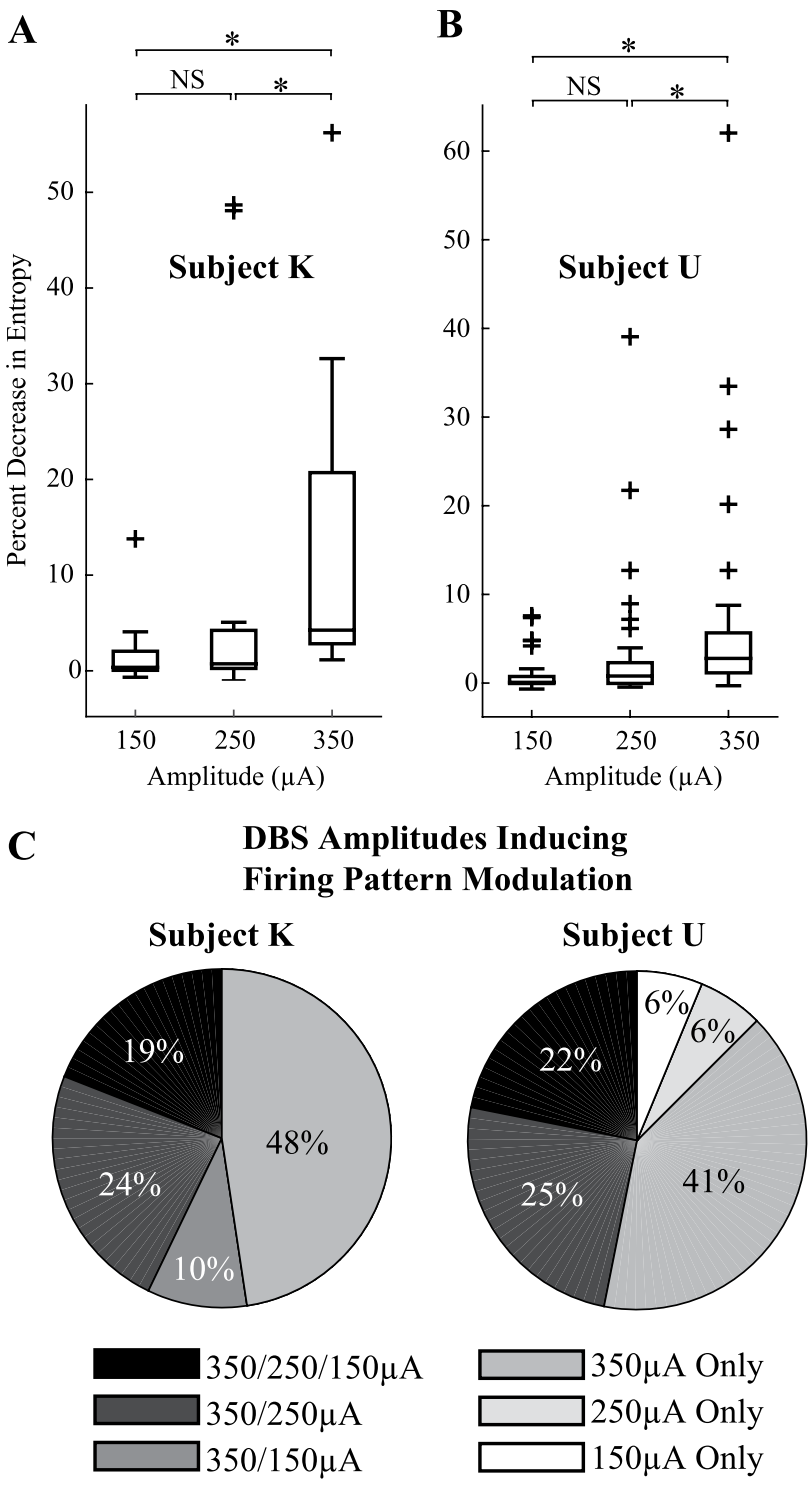

Figure 4. Effect of HFS amplitude on PSTH entropy change and firing pattern modulation. (**A,B**) Shown are population-based entropy changes in those cells with at least one significant entropy change amongst the three stimulus amplitudes. NS: no significant difference by multiple comparison test. *Significant difference by Mann-Whitney U test with Bonferroni correction ($\alpha = 0.0167$, FPM cells: Subject K, n = 21 recordings; Subject U, n = 32 recordings). (**C**) Likelihood of firing pattern modulation to occur across the three different stimulus amplitudes.

Discussion

The results of this study indicate that there is substantial heterogeneity in local neuronal responses to motor thalamic HFS, including modulation of firing rate and pattern across populations of neurons within motor thalamus. Further, the volume of tissue modulated in terms of firing pattern around the implanted DBS array was sparsely

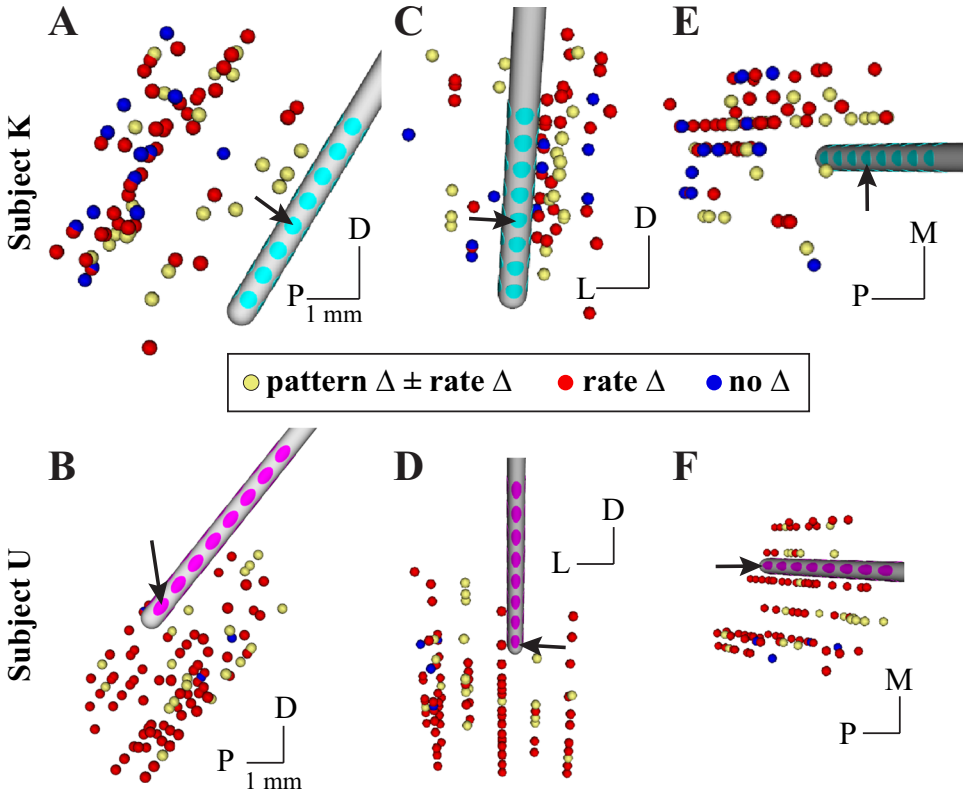

Figure 5. Distribution of modulated motor thalamic activity with respect to microdrive-defined recording site location. Recording location sphere colors correspond to whether no modulation was observed for any stimulus setting (blue), only a change in firing rate was observed (red), and if a firing pattern change was observed regardless of whether or not a rate change was also observed (yellow). Perspectives are shown for sagittal (**A**,**B**) coronal (**C**,**D**) and axial (**E**,**F**) perspectives in both subjects. D: dorsal; P: posterior; L: lateral; M: medial. Scale bars indicates 1-mm.

populated and not confined to the immediate vicinity of the active electrode. Increasing stimulation amplitudes induced both a greater change in the strength of the firing pattern entropy difference as well as recruited a denser population of motor thalamic neurons within the volume of tissue modulated. Previous studies have mostly characterized thalamic neuronal responses to short duration intrathalamic stimulation[12,29,47–49] with fewer studies investigating intrathalamic effects on the order of 10 s of seconds[50,51]. The data presented in this study also expand on the spatiotemporal changes in neuronal spike activity that occur during longer duration HFS within the motor thalamus.

HFS induced primarily firing rate modulation and in particular a decreased spike rate without complete cessation of spike activity *during* HFS. These findings extend previous reports showing that the major effect *following* short periods of thalamic stimulation was local depression of neuronal activity characterized by complete silencing of neuronal spike activity[52] or more complex burst patterns followed by quiescent periods that depended on stimulation parameters[12]. Firing pattern modulation was observed less frequently with 'p+' type responses being most common in both subjects. The relative difference in firing rate versus pattern modulation may stem in part from the prevalence or strength of excitatory relative to inhibitory inputs within VPLo thalamus[10,11,16]. Moreover, the results may also stem from the ability of HFS to more readily modulate specific axonal afferent and efferent processes based upon the relative orientation of the electric field to the axonal trajectories within motor thalamus[53].

The majority of recordings showed that neuronal activity was not widely influenced by all HFS settings. These findings are consistent with previous reports, where 55%[47] and 51%[49] of motor thalamic neurons were unaffected by stimulation following brief (0.5 ms) periods of stimulation with amplitudes ranging from 120–200 µA. It is important to note, however, that increasing stimulation amplitude in our study was found to result in greater firing pattern modulation at the expense of firing rate modulation alone. For cells exhibiting firing pattern modulation at any one of the stimulation amplitudes, the results showed a stronger degree of firing pattern modulation for a given cell with increasing stimulation amplitude. This difference in modulatory effect was found between 250–350 µA and not between 150–250 µA, suggesting a nonlinear recruitment effect with stimulation amplitude. Together, these results suggest that additional increases in stimulation amplitude may further shift the population responses and the strength of the modulatory effect from one primarily based on firing rate modulation to one showing a broad class of firing rate and pattern modulation within motor thalamus. The clinical implication for these results is that, at lower stimulation amplitudes, the mechanism of 'de-rhythmication'[51] may involve

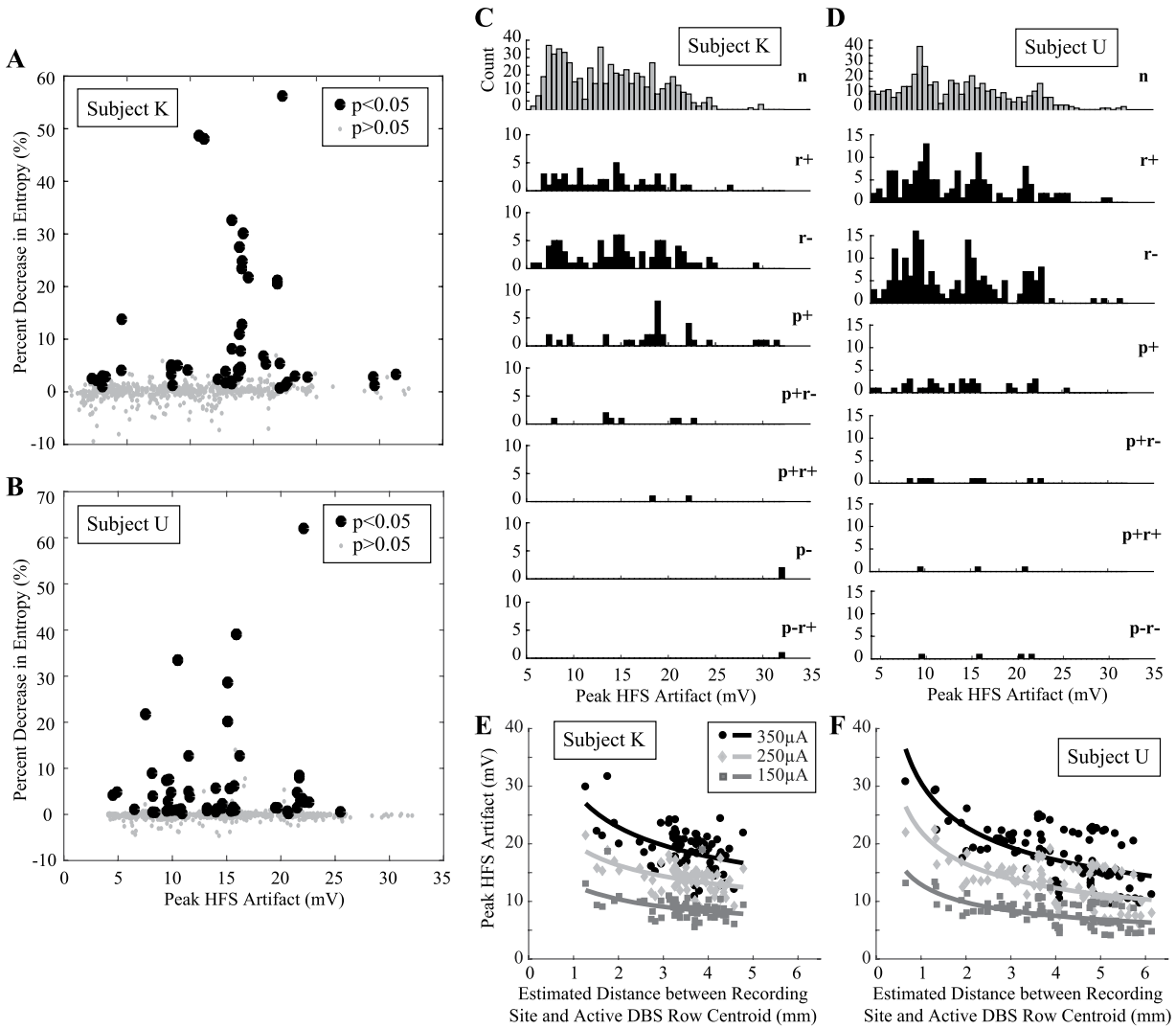

Figure 6. Distribution of modulated motor thalamic activity with respect to stimulation artifact size. Percent decrease in PSTH entropy between the HFS-off and HFS-on periods plotted against the peak amplitude of the recorded HFS artifact for (**A**) Subject K and (**B**) Subject U. Recordings that exhibited significant firing pattern modulation during HFS are labeled as large black solid circles. (**C**,**D**) Spatial distribution of neuronal recordings grouped by their response to HFS (p: firing pattern modulation, r: firing rate modulation. '+': increase in firing rate or phase-locked spike activity, '−': decrease in firing rate or phase-locked spike activity, n: no response). (**E**,**F**) Relationship between the stimulus artifact peak amplitude and the estimated recording site distance from the centroid point of the active DBS row. Shown are data for both subjects categorized based on stimulus amplitude (150, 250, and 350 µA).

'masking' rhythmic tremor activity within thalamus[54] by creating noise in the population spike activity (for firing rate increases) or by raising the threshold for propagation of tremor burst activity (for firing rate decreases). At higher stimulus amplitudes, however, the results indicate that the mechanism shifts to disruption of tremor activity within thalamus via firing pattern modulation of spike activity, which is known to induce information lesions[1].

The recording data also showed that instances of significant firing rate and pattern modulation occurred over a wide range of distances that were not confined to the immediate vicinity of the active electrode. This resulted in neuronal response subtypes for any given stimulation setting being sparsely distributed around the DBS array. This sparse distribution of modulated neurons is consistent with observations from other studies. Following brief stimulation in the ventrolateral nucleus (VPLo homologue) in cats, non-responsive cells were reported to be widely distributed, even very close (<1 mm) to the stimulating electrode[52]. Similar sparse and distributed spatial modulation profiles have also been observed in the visual cortex using two-photon calcium imaging[26]. Interestingly, the variation in the ΔH% observed amongst the modulated cells that we observed in our study (Fig. 6) may also represent the underlying phenomenon visualized with calcium imaging as a difference in fluorescence intensity of activated cells[26]. One explanation for both the heterogeneous responses and the distributed spatial modulation profiles is that electrical stimulation results in very local excitation of axons, which pass adjacent to the active electrode. The afferents and efferents within motor thalamus are known to have diverse

branching patterns and trajectories[55], and driving action potentials within these axons would result in a complex set of antidromic and orthodromic responses within motor thalamus consistent with the observations from this study.

There are several considerations in interpretation of the results, including that the data were not collected in a disease model. Harmaline treatment is the most established model to induce action tremor[56]; however, harmaline-induced tremor is transient and studies have shown that animals develop resistance to the treatment[57,58] making it impractical for the experimental protocols conducted in this study. Future studies that leverage multi-channel electrode arrays in conjunction with harmaline treatment and a movement task will be important to validate the results of this study in the context of action tremor. Another study limitation is the size of the stimulation artifact as a pseudo-measure of distance between recorded neurons to the stimulating electrode. This approach was implemented because exact Euclidian distances were not readily available from histology in the two subjects. However, the relationship between the peak stimulus artifact amplitude and the estimated distance from the corresponding recording site location and the row of active DBS showed a nonlinear decay function that was consistent with that reported previously[43]. Variation in the curve fitting could stem from slight discrepancies in the estimated site locations from the microdrive coordinate system as well as shadowing that may occur between electrodes active on one side of the DBS lead and recording sites performed on the other side of the DBS lead. Finally, the range of stimulation amplitudes investigated in this study was relatively small in scope. However, the data point towards larger stimulation amplitudes further increasing the percentage of cells modulated and further increasing the percentage of responses identified as firing pattern modulation.

As far as we know, this study is the first of a kind effort to map the distribution of various HFS-induced changes in neuronal activity around a chronically implanted DBS array. Motor thalamus unit-spike recordings exhibited several classes of firing rate and firing pattern responses to locally-applied HFS with broad spatial distributions. Increasing stimulation amplitude was found to non-linearly increase the modulation volume density but also shift the type of modulation from one based primarily on firing rate modulation to one based in greater measure on firing pattern modulation. Together, these mechanistic findings have important implications for computational models of DBS[11,59–62], closed-loop stimulation therapies[62], as well as development of targeting approaches to more selectively modulate deep brain cellular pathways[11,59,61,63].

References

1. Agnesi, F., Connolly, A. T., Baker, K. B., Vitek, J. L. & Johnson, M. D. Deep brain stimulation imposes complex informational lesions. *PloS one* **8**, e74462, https://doi.org/10.1371/journal.pone.0074462 (2013).
2. Grill, W. M., Snyder, A. N. & Miocinovic, S. Deep brain stimulation creates an informational lesion of the stimulated nucleus. *Neuroreport* **15**, 1137–1140 (2004).
3. Chiken, S. & Nambu, A. High-frequency pallidal stimulation disrupts information flow through the pallidum by GABAergic inhibition. *The Journal of neuroscience: the official journal of the Society for Neuroscience* **33**, 2268–2280, https://doi.org/10.1523/JNEUROSCI.4144-11.2013 (2013).
4. Filali, M., Hutchison, W. D., Palter, V. N., Lozano, A. M. & Dostrovsky, J. O. Stimulation-induced inhibition of neuronal firing in human subthalamic nucleus. *Experimental brain research. Experimentelle Hirnforschung* **156**, 274–281 (2004).
5. Boraud, T., Bezard, E., Bioulac, B. & Gross, C. High frequency stimulation of the internal Globus Pallidus (GPi) simultaneously improves parkinsonian symptoms and reduces the firing frequency of GPi neurons in the MPTP-treated monkey. *Neurosci Lett* **215**, 17–20 (1996).
6. Dostrovsky, J. O. *et al*. Microstimulation-induced inhibition of neuronal firing in human globus pallidus. *J Neurophysiol* **84**, 570–574 (2000).
7. Bar-Gad, I., Elias, S., Vaadia, E. & Bergman, H. Complex locking rather than complete cessation of neuronal activity in the globus pallidus of a 1-methyl-4-phenyl-1,2,3,6-tetrahydropyridine-treated primate in response to pallidal microstimulation. *J Neurosci* **24**, 7410–7419 (2004).
8. Meissner, W. *et al*. Subthalamic high frequency stimulation resets subthalamic firing and reduces abnormal oscillations. *Brain* **128**, 2372–2382 (2005).
9. Kuncel, A. M., Cooper, S. E., Wolgamuth, B. R. & Grill, W. M. Amplitude- and frequency-dependent changes in neuronal regularity parallel changes in tremor With thalamic deep brain stimulation. *IEEE transactions on neural systems and rehabilitation engineering: a publication of the IEEE Engineering in Medicine and Biology Society* **15**, 190–197, https://doi.org/10.1109/TNSRE.2007.897004 (2007).
10. Birdno, M. J., Cooper, S. E., Rezai, A. R. & Grill, W. M. Pulse-to-pulse changes in the frequency of deep brain stimulation affect tremor and modeled neuronal activity. *Journal of neurophysiology* **98**, 1675–1684, https://doi.org/10.1152/jn.00547.2007 (2007).
11. McIntyre, C. C., Grill, W. M., Sherman, D. L. & Thakor, N. V. Cellular effects of deep brain stimulation: model-based analysis of activation and inhibition. *J Neurophysiol* **91**, 1457–1469 (2004).
12. Birdno, M. J., Tang, W., Dostrovsky, J. O., Hutchison, W. D. & Grill, W. M. Response of human thalamic neurons to high-frequency stimulation. *PloS one* **9**, e96026, https://doi.org/10.1371/journal.pone.0096026 (2014).
13. Ando, N., Izawa, Y. & Shinoda, Y. Relative contributions of thalamic reticular nucleus neurons and intrinsic interneurons to inhibition of thalamic neurons projecting to the motor cortex. *Journal of neurophysiology* **73**, 2470–2485 (1995).
14. Asanuma, C., Thach, T. & Jones, E. G. Distribution of cerebellar terminations in the ventral lateral thalamic region of the monkey. *Brain Res.Rev.* **5**, 237–265 (1983).
15. Sherman, S. M. & Guillery, R. W. Functional organization of thalamocortical relays. *J Neurophysiol* **76**, 1367–1395 (1996).
16. Jones, E. G. *The Thalamus*. (Plenum Press, 1985).
17. Hamani, C., Dostrovsky, J. O. & Lozano, A. M. The motor thalamus in neurosurgery. *Neurosurgery* **58**, 146–158; discussion 146–158 (2006).
18. Anderson, T., Hu, B., Pittman, Q. & Kiss, Z. H. Mechanisms of deep brain stimulation: an intracellular study in rat thalamus. *The Journal of physiology* **559**, 301–313, https://doi.org/10.1113/jphysiol.2004.064998 (2004).
19. Chomiak, T. & Hu, B. Axonal and somatic filtering of antidromically evoked cortical excitation by simulated deep brain stimulation in rat brain. *The Journal of physiology* **579**, 403–412 (2007).
20. Lee, K. H. *et al*. High frequency stimulation abolishes thalamic network oscillations: an electrophysiological and computational analysis. *J Neural Eng* **8**, 046001, https://doi.org/10.1088/1741-2560/8/4/046001 (2011).
21. Lee, K. H. *et al*. Abolition of spindle oscillations and 3-Hz absence seizurelike activity in the thalamus by using high-frequency stimulation: potential mechanism of action. *Journal of neurosurgery* **103**, 538–545, https://doi.org/10.3171/jns.2005.103.3.0538 (2005).

22. Agnesi, F., Blaha, C. D., Lin, J. & Lee, K. H. Local glutamate release in the rat ventral lateral thalamus evoked by high-frequency stimulation. *J Neural Eng* **7**, 26009, https://doi.org/10.1088/1741-2560/7/2/026009 (2010).
23. Bekar, L. *et al*. Adenosine is crucial for deep brain stimulation-mediated attenuation of tremor. *Nature medicine* **14**, 75–80, https://doi.org/10.1038/nm1693 (2008).
24. Chang, S. Y. *et al*. Wireless fast-scan cyclic voltammetry to monitor adenosine in patients with essential tremor during deep brain stimulation. *Mayo Clinic proceedings* **87**, 760–765, https://doi.org/10.1016/j.mayocp.2012.05.006 (2012).
25. Ranck, J. B. Jr. Which elements are excited in electrical stimulation of mammalian central nervous system: a review. *Brain research* **98**, 417–440 (1975).
26. Histed, M. H., Bonin, V. & Reid, R. C. Direct activation of sparse, distributed populations of cortical neurons by electrical microstimulation. *Neuron* **63**, 508–522 (2009).
27. Xiao, Y. *et al*. Multimodal 7T imaging of thalamic nuclei for preclinical deep brain stimulation applications. *Frontiers in neuroscience* **10**, https://doi.org/10.3389/fnins.2016.00264 (2016).
28. Miocinovic, S., Noecker, A. M., Maks, C. B., Butson, C. R. & McIntyre, C. C. Cicerone: stereotactic neurophysiological recording and deep brain stimulation electrode placement software system. *Acta Neurochir Suppl* **97**, 561–567 (2007).
29. Vitek, J. L., Ashe, J., DeLong, M. R. & Kaneoke, Y. Microstimulation of primate motor thalamus: somatotopic organization and differential distribution of evoked motor responses among subnuclei. *J Neurophysiol* **75**, 2486–2495 (1996).
30. Connolly, A. T. *et al*. A novel lead design for modulation and sensing of deep brain structures. *IEEE transactions on bio-medical engineering* **63**, 148–157, https://doi.org/10.1109/TBME.2015.2492921 (2016).
31. Lempka, S. F., Johnson, M. D., Miocinovic, S., Vitek, J. L. & McIntyre, C. C. Current-controlled deep brain stimulation reduces *in vivo* voltage fluctuations observed during voltage-controlled stimulation. *Clin Neurophysiol* **121**, 2128–2133, https://doi.org/10.1016/j.clinph.2010.04.026 (2010).
32. Wharen, R. E. *et al*. *Thalamic DBS with a constant-current* device in essential tremor: A controlled clinical trial. Parkinsonism & related disorders ((in press)).
33. Mai, J. r. K., Assheuer, J. & Paxinos, G. *Atlas of the human brain*. 2nd edn, (Elsevier Academic Press, 2004).
34. Paxinos, G., Huang, X. F. & Toga, A. W. *The rhesus monkey brain in stereotaxic coordinates*. (Academic Press, 2000).
35. Hashimoto, T., Elder, C. M. & Vitek, J. L. A template subtraction method for stimulus artifact removal in high-frequency deep brain stimulation. *Journal of neuroscience methods* **113**, 181–186 (2002).
36. Agnesi, F., Muralidharan, A., Baker, K. B., Vitek, J. L. & Johnson, M. D. Fidelity of frequency and phase entrainment of circuit-level spike activity during DBS. *Journal of neurophysiology* **114**, 825–834, https://doi.org/10.1152/jn.00259.2015 (2015).
37. Dorrscheidt, G. H. The statistical significance of the peristimulus time histogram (PSTH). *Brain Res* **220**, 397–401 (1981).
38. Selinger, J. V., Kulagina, N. V., O'Shaughnessy, T. J., Ma, W. & Pancrazio, J. J. Methods for characterizing interspike intervals and identifying bursts in neuronal activity. *Journal of neuroscience methods* **162**, 64–71, https://doi.org/10.1016/j.jneumeth.2006.12.003 (2007).
39. Dorval, A. D. Probability distributions of the logarithm of inter-spike intervals yield accurate entropy estimates from small datasets. *Journal of neuroscience methods* **173**, 129–139, https://doi.org/10.1016/j.jneumeth.2008.05.013 (2008).
40. Dorval, A. D. Estimating Neuronal Information: Logarithmic Binning of Neuronal Inter-Spike Intervals. *Entropy* **13**, 485–501, https://doi.org/10.3390/e13020485 (2011).
41. Strong, S. P., Koberle, R., van Steveninck, R. R. D. & Bialek, W. Entropy and information in neural spike trains. *Phys Rev Lett* **80**, 197–200, https://doi.org/10.1103/PhysRevLett.80.197 (1998).
42. Shannon, C. E. & Weaver, W. *The mathematical theory of communication*. (University of Illinois press, 2015).
43. Miocinovic, S. *et al*. Experimental and theoretical characterization of the voltage distribution generated by deep brain stimulation. *Experimental neurology* **216**, 166–176 (2009).
44. Plonsey, R. & Heppner, D. B. Considerations of quasi-stationarity in electrophysiological systems. *The Bulletin of mathematical biophysics* **29**, 657–664 (1967).
45. Harris, K. D., Henze, D. A., Csicsvari, J., Hirase, H. & Buzsaki, G. Accuracy of tetrode spike separation as determined by simultaneous intracellular and extracellular measurements. *Journal of Neurophysiology* **84**, 401–414 (2000).
46. Henze, D. A. *et al*. Intracellular features predicted by extracellular recordings in the hippocampus *in vivo*. *J Neurophysiol* **84**, 390–400 (2000).
47. Marco, L., Brown, T. & Rouse, M. Unitary responses in ventrolateral thalamus upon intranuclear stimulation. *J Neurophys* **30**, 482–493 (1967).
48. Sakata, H., Ishijima, T. & Toyoda, Y. Single unit studies on ventrolateral nucleus of the thalamus in cat: its relation to the cerebellum, motor cortex and basal ganglia. *The Japanese journal of physiology* **16**, 42–60 (1966).
49. Schlag, J. & Villablanca, J. A quantitative study of temporal and spatial response patterns in a thalamic cell population electrically stimulated. *Brain Res* **8**, 255–270 (1968).
50. Kent, A. R. & Grill, W. M. Neural origin of evoked potentials during thalamic deep brain stimulation. *J Neurophys* **110**, 826–843 (2013).
51. Kiss, Z. H., Mooney, D. M., Renaud, L. & Hu, B. Neuronal response to local electrical stimulation in rat thalamus: physiological implications for mechanisms of deep brain stimulation. *Neuroscience* **113**, 137–143 (2002).
52. Schlag, J. & Villablanca, J. Thalamic inhibition by thalamic stimulation. *Psychonomic Science* **8**, 373–374 (1967).
53. Lehto, L. J. *et al*. Orientation selective deep brain stimulation. *J Neural Eng* **14**, 016016, https://doi.org/10.1088/1741-2552/aa5238 (2017).
54. Lenz, F. A. *et al*. Tremor-related activity in functionally identified cells. *Brain: a journal of neurology* **117**(Pt 3), 531–543 (1994). Single unit analysis of the human ventral thalamic nuclear group.
55. Jones, E. G. *The thalamus*. 2nd edn, (Cambridge University Press, 2007).
56. Elble, R. J. Animal models of action tremor. *Mov Disord* **13**(Suppl 3), 35–39 (1998).
57. Lutes, J., Lorden, J. F., Beales, M. & Oltmans, G. A. Tolerance to the tremorogenic effects of harmaline: evidence for altered olivo-cerebellar function. *Neuropharmacology* **27**, 849–855 (1988).
58. Miwa, H. Rodent models of tremor. *Cerebellum* **6**, 66–72, https://doi.org/10.1080/14734220601016080 (2007).
59. Keane, M., Deyo, S., Abosch, A., Bajwa, J. A. & Johnson, M. D. Improved spatial targeting with directionally segmented deep brain stimulation leads for treating essential tremor. *J Neural Eng* **9**, 046005, https://doi.org/10.1088/1741-2560/9/4/046005 (2012).
60. Kuncel, A. M., Birdno, M. J., Swan, B. D. & Grill, W. M. Tremor reduction and modeled neural activity during cycling thalamic deep brain stimulation. *Clinical neurophysiology: official journal of the International Federation of Clinical Neurophysiology* **123**, 1044–1052, https://doi.org/10.1016/j.clinph.2011.07.052 (2012).
61. Kuncel, A. M., Cooper, S. E. & Grill, W. M. A method to estimate the spatial extent of activation in thalamic deep brain stimulation. *Clinical neurophysiology: official journal of the International Federation of Clinical Neurophysiology* **119**, 2148–2158, https://doi.org/10.1016/j.clinph.2008.02.025 (2008).
62. Santaniello, S., Fiengo, G., Glielmo, L. & Grill, W. M. Closed-loop control of deep brain stimulation: a simulation study. *IEEE transactions on neural systems and rehabilitation engineering: a publication of the IEEE Engineering in Medicine and Biology Society* **19**, 15–24, https://doi.org/10.1109/TNSRE.2010.2081377 (2011).
63. Yousif, N. *et al*. A network model of local field potential activity in essential tremor and the impact of deep brain stimulation. *PLoS computational biology* **13**, e1005326, https://doi.org/10.1371/journal.pcbi.1005326 (2017).

Acknowledgements

This work was supported by the National Institutes of Health under grants R01-NS081118 and R01-NS094206, and by a MnDRIVE fellowship (to YX). We thank Rio Vetter, Jamie Hetke, KC Kong, and Rob Shoemaker from Neuronexus Technologies for helping with the design and fabrication of the DBS arrays. We thank Noam Harel, Essa Yacoub, and Gregor Adriany at the Center for Magnetic Resonance Research for assistance with the imaging (NIH P41-EB015894, P30-076408, U54-MH091657). We also thank Kenneth Baker for helpful discussion, and thank Alexandra Doyle, Edgar Peña, Julia Slopsema, Logan Grado, and Nate Faber for help with the experiments.

Author Contributions

Y.X., J.L.V., and M.D.J. designed the study. Y.X., F.A., E.M.B., S.Z. and M.D.J. performed the experiments. Y.X. and M.D.J. analyzed the results and wrote the paper.

Additional Information

Competing Interests: The authors declare that they have no competing interests.

Publisher's note: Springer Nature remains neutral with regard to jurisdictional claims in published maps and institutional affiliations.